Homework Four Individual Analysis

Chyler Bitsoi
22 November 2025
Active Rocket Control
Active Fin Servo Mechanism
ME 476C - Section 001

Fall 2025-Spring 2026

1.0 Introduction:

The Active Rocket Control (ARC) System aims to command roll stabilization for a high-powered 3-inch class rocket in flight. The goal of this team is to actively generate, stop, and stabilize a commanded roll rate of approximately ±100 RPM through active stabilization using the aerodynamic control surfaces of the aft fins and nose cone driven by an internal servo and pushrod mechanism. Since these forces are encountered under substantial dynamic pressure, mechanical integrity of the servo, linkages and hinge assembly must be validated for the design to progress towards fabrication and testing.

This report documents the analytical assessment of the aft-fin actuation system focusing on required servo torques, hinge moment loading, and assessment of the pushrod from the internal servo providing torque to the external fins. The aerodynamic forces on the control surfaces are derived from theoretical considerations based on geometric dimensions of the fins, their center-of-pressure location and anticipated velocities during flight from RockSim assessment. These loads are converted through a free-body analysis of the fin and horn and servo arm to establish required servo input torque and axial and bending loads sustained by the pushrod. Finally, the analysis is validated through mechanics-of-materials assessments and machine design requirements to ensure a successful actuation mechanism relative to operation and safety requirements. Pushrod material options (PLA, Aluminum) are assessed relative to allowable stresses, buckling potential, and final factor of safety for worst case loading which supports servo selection as well as linkage material to provide optimal reliability during expected conditions over the mission envelope.

2.0 Assumptions:

The assumptions made below are necessary to characterize the aerodynamic loads, servo-linkage loads, and fin-actuation pushrod structural strength of the active rocket control system according to industry-accepted norms of aerodynamics, statics, material science, and machine design.

2.1 Flight Aerodynamics:

2.1.a. The dynamic pressure used in Eq.3 uses Rocksim predicts a maximum ascent velocity of 1150 ft/s under expected launch conditions. Using standard low-altitude air density $\rho = 0.0020\ slug/ft^3$. This assumption is consistent with NASA atmospheric properties [3]. This pressure corresponds to the maximum aerodynamic loading that the fins will experience while moving upwards around max-Q. By utilizing the maximum dynamic pressure in worst-case scenarios, the device can maintain structural integrity for maximum levels of aerodynamics.

2.1.b. The lift coefficient used in Eq.1 is assumed to vary linearly with angle of attack per airfoil theory with slope $C_{l\alpha} = 2\pi\ per\ rad$ as seen in aerodynamic texts [1], and [2]. This assumption is valid within our active rocket design since our project rocket will use relatively small fin deflection preventing nonlinear stall behavior.

2.1.c. The aerodynamic normal force of Eq. (4) is assumed quasi-steady and incompressible. However, since Mach number reaches transonic conditions at maximum speed, the compressibility of hinge-moment is not as sensitive as its dependence to dynamic pressure, allowing this assumption for structural modeling purposes.

21.d. The moment arm xcp used in Eq. (5) is taken from the theory that the fin aerodynamic center is located at ~35% of mean aerodynamic chord, as per Barrowman's low-aspect-ratio rocket fin aerodynamic stability model [5]. This location has significant, reliable correlation for model rockets and generates an adequate approximation of hinge moment.

2.2 Fin Deflection/Geometry:

2.2.a The fin area calculated via Eq. (2) is based on a trapezoidal, rigid geometry based off of the RockSim/CAD dimensions. Aeroelastic deformation does not come into play because the fins are rigid enough and small enough displacements mean deflection is negligible.

2.2.b All aerodynamic equations and Eqs. (1), (4) and (5) assume that the fin deflections stay within the small-angle regime. This means that lift, hinge moment and force calculations are linear and consistent with thin-airfoil assumptions [1].

2.2.c The distance between the fin and fin-horn mounting point occurs approximately one-third into the semi-span from the edge of the fin tip. This measurement is taken into consideration for Eq. (6) to determine how much pushrod force can be exerted from a measured hinge moment. This is based upon internal clearance and anticipated structural stiffness; placement will be optimized in future works.

2.3 Servo and linkage mechanism:

2.3.a. The stall torque T_{stall} referenced in Eq. (8) and Eq. (9) comes from the manufacturer's specifications for the KST X15-755X [7]. This is considered an absolute mechanical boundary - meaning that regardless of aerodynamic effort needed, the pushrod force will not exceed that of Eq. (9).

2.3.b. The servo horn and the fin horn are each considered rigid bodies and the linkage geometry is ideal without any backlash or elastic deformation. Thus, Eq. (6) and Eq. (9) can be implemented using simple moment-arm relationships according to standard servo-mechanism modeling procedures [8].

2.3.c. Servo torque is independent of speed, friction, and heating. This is an ultimate load condition since in dynamic actuation, such magnitude would be reduced due to true torque losses due to friction and dynamic movements. This is a conservative measure for structural loading

2.4 Pushrod Material and structural behavior:

2.4.a. The axial stress relation used in Eq. (11) is a linearly elastic assumption since both aluminum and PLA operate in linearly elastic ranges. This is true of mechanics-of-materials equations for axially loaded conditions [6].

2.4.b. The material properties from [9] include PLA and aluminum 6061-T6. The assumption of isotropy is valid for both materials; albeit, PLA prints are sometimes anisotropic. It's more convenient to assume homogeneous and isotropic since the analysis variables provide conservative (lowered) strengths.

2.4.c. The slenderness ratio of the pushrod means that the compressive failure of interest will be the Euler column buckling relation. The assumption in Eq. (12) is a pinned - pinned rod which is appropriate since the clevis-rod geometry in the linkage operates as such [6].

2.4.d. The diameter used for the area moment of inertia from Eq. (13) is measured from the CAD render as are the fixed lengths:
Diameter = 1/8 in
Unsupported length = ~10.16 in
These are crucial since they determine the buckling strength.

3.0 Physical Modeling:

The physical system abstracted for this model is the ARC unit assembly actuating each aft fin, comprising the fin, hinge, and servo-driven pushrod. Each fin is modeled as a rigid trapezoidal plate where the planform area and mean aerodynamic chord comes from RockSim/CAD geometry. Each fin also connects to the airframe through a hinge line at its root, such that any aerodynamic loading generated on the surface generates a hinge moment about this axis. The aerodynamic center is located at 35% of the mean aerodynamic chord, which is the distance between the hinge axis and aerodynamic center generating the moment from fin normal force.

From a mechanical perspective, the fins connect internally to a servo by means of a rigid horn and straight pushrod. The rigid fin horn is modeled as a lever arm of length from the hinge axis to the point at which it connects to a straight rigid pushrod. This pushrod experiences a magnitude of force equal to, where the moment about the hinge from the adjacent hinge moment is equal to simply obtained through a moment equilibrium relation. In addition, since the rod connects to the servo side horn radius at a defined radius, that provides an indirect means of taking servos stall torque and converting it to an equivalent axial load in the pushrod in a manner where it serves as a maximum for any force acting in the linkage assembly. Finally, the pushrod is idealized as a straight solid circular bar with axial loading. It is simply supported by pinned joints at either end; with buckling, it has a slenderness ratio sufficiently small enough for Euler column pinned-pinned modeling relevant to buckling analysis

4.0 Models Schematics:

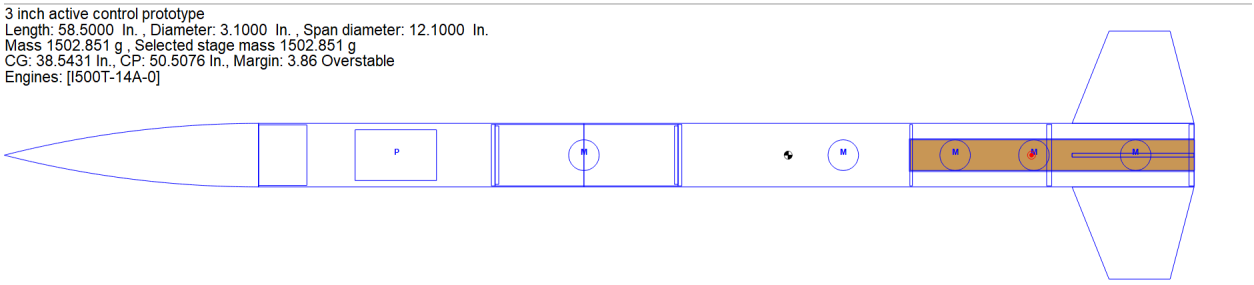

Figure 1: Rocksim Schematic

Simulation	Engine diameter(s) mm	Results	Altitude at deployment Feet	Engines loaded	Max. altitude Feet	Max. velocity Feet / Sec	Time to apogee	Time to burnout	Velocity at deployment Feet / Sec
0	38		5366.83	[I500T-14A-14]	5369.26	948.97	15.71	1.34	25.58
1	38		5361.58	[I500T-14A-14]	5363.91	948.82	15.71	1.34	24.96
2	38		5562.20	[I500T-14A-0]	5562.20	1199.16	15.08	1.34	52.45
3	38		5609.71	[I500T-14A-0]	5609.71	1199.66	15.16	1.34	40.57
4	38		5509.38	[I500T-14A-0]	5509.38	1198.58	15.00	1.34	62.88
5	38		5515.81	[I500T-14A-0]	5515.81	1198.65	15.01	1.34	61.72
6	38		5590.81	[I500T-14A-0]	5590.81	1199.47	15.13	1.34	45.70
7	38		5517.78	[I500T-14A-0]	5517.78	1198.67	15.01	1.34	61.36

Figure 2: Rocksim simulation results

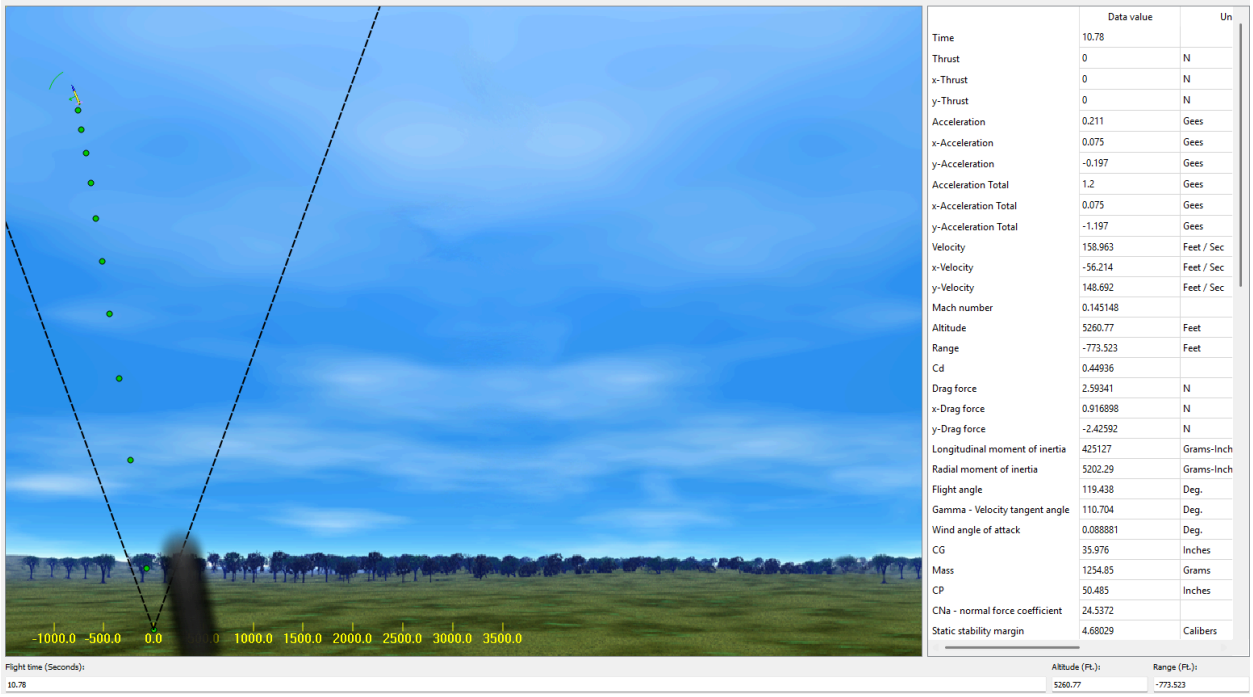

Figure 3: Rocksim simulated flight results

5.0 Analytical Modeling:

The below analysis derives the aerodynamic loads on the fin, hinge moment, pushrod force to turn the fin, and pushrod loading. All governing equations are rooted in classical aerodynamics, statics, and mechanics of materials and numbered for convenience.

5.1 Aerodynamic Forces:

The aerodynamic lift coefficient for small angles of fin deflection is approximated as perpendicular to flow by thin air foil theory.

$$C_l = C_l\delta \quad (1)$$

Where $C_l = 2\,\pi\, rad$ For low aspect ratio fins, the fin platform area is integrated over the trapezoid shape.

$$S = \frac{(c_r + c_t)}{2} \quad (2)$$

The dynamic pressure is assumed as the same dynamic pressure experienced at maximum ascent velocity.

$$q_{max} = \frac{1}{2}\rho V^2 \quad (3)$$

Where rocksim anticipated V = 1150 ft/s and for low altitude $\rho = 0.0020\ slug/ft^3$. The lift generated on the fin due to the aerodynamic coefficient is then given by:

$$L = qSC_l \quad (4)$$

Which applies a moment about the root of the fin with:

$$M_h = Lx_{cp} \quad (5)$$

Where x_{cp} is the distance from the hinge to the geometric center assumed to be 35% of mean aerodynamic chord [5].

5.2 Pushrod force:

The moment must be reacted through the fin horn by the pushrod and by assuming the moment equilibrium from static bounds:

$$M_h = F_{rod} r_f \quad (6)$$

The effective force delivered by the pushrod becomes:

$$F_{rod} = \frac{M_h}{r_f} \quad (7)$$

which delivers demand, not necessarily force, as a servo can limit that enforceable requirement.

5.3 Servo Motor Force:

The selected servo, KST X15-755X, comes with a stall torque:

$$T_{stall} = 8.85\ lbf \quad (8)$$

Thus, the maximum force generated by the pushrod of the servo comes from:

$$F_{rod,max} = \frac{T_{stall}}{r_s} \quad (9)$$

which assumes hole usage at either end of the push rod attachment to the servo horn where r s is the horn radius. This value represents the absolute maximum compressive or tensile load that can be transmitted through the pushrod, independently of aerodynamic requirements [7],[8].

5.4 Axial Stress in pushrod:

The pushrod is approximated as a solid cylinder bar of diameter d. Its cross sectional area can be modeled as:

$$A = \frac{\pi d^2}{4} \quad (10)$$

The axial stress in the pushrod due to the transmitted force is:

$$\sigma = \frac{F}{A} \quad (11)$$

This stress is compared to material tensile (PLA) or yield strength (Aluminum 6061-T6)

5.5 Buckling Check (Euler):

Due to the pushrod slenderness with pinned ends, compressive failure is governed by Euler buckling. The critical load is modeled as:

$$P_{cr} = \frac{\pi EI}{(KL)^2} \quad (12)$$

The second moment of area for a circular rod is:

$$I = \frac{\pi d^4}{64} \quad (13)$$

This formula is appropriate because the effective length factor for a pinned-pinned column is K = 1 [6].

5.6 Pin and Joint Sheer:

Clevis pins at the rod ends are loaded in double shear. The corresponding stress can be modeled as:

$$\tau = \frac{F}{2A_p} \quad (14)$$

Pin sheer is evaluated to confirm that the joint hardware is not a limiting factor in the design [10].

6.0 Solidworks CAD model:

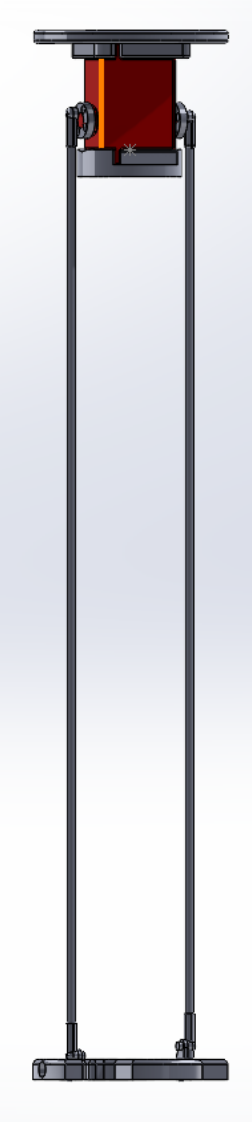

Figure 4: Front View

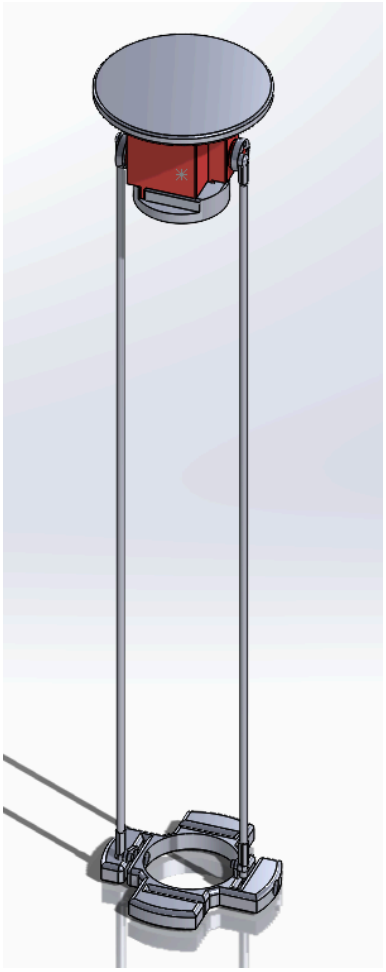

Figure 5: isometric view

7.0 Results:

The analytical model from Section 3 was utilized to assess the aerodynamic hinge moment, resultant pushrod force and structural integrity of the two pushrod materials: PLA and aluminum. Flight data from RockSim was extrapolated to determine the worst-case aerodynamic scenario. Maximum ascent velocity approached 1150 ft/s which corresponds to a maximum dynamic pressure just under 1300 psf at standard low density at low altitude. Plugging this value into the equations for aerodynamic lift and hinge moment yielded a resultant fin normal force and hinge moment that were both well below the stall torque limit of the KST X15-755X servo. While the aerodynamic loading on the control fins surely increases significantly at max-Q, the resultant calculated hinge moment is never above the servo's stall torque limit. Thus, it can be concluded that the KST X15-755X servo will limit any pushrod force before the aerodynamic environment will. This is a good outcome because it minimizes uncertainty in worst-case load determination and allows for determination of maximum pushrod force through servo geometry as opposed to an aerodynamically induced variance.

Using the stall torque of 8.85 lbf determined from the KST X15-755X sub-assemblies and the measured distance from the servo shaft axis to horn coupling radius, the maximum pushrod force transmitted fell within the range of 17 to 22 lbf, dependent on which horn length was set during assembly. This

servo-limited value was used as the governing condition for all structural checks performed. The aerodynamic contribution was maintained for thoroughness, but it ultimately is below the servo-limited value and therefore does not dictate design evaluation.

To assess axial stress within the pushrod, the associated load was placed over the cross-sectional area of a 1/8-in solid rod. For the maximum estimated force from the servo, resultant axial stresses equate to about 1400 to 1800 psi. Compared against material strengths, where aluminum 6061-T6 satisfies axial stress requirements with a large safety factor (yielding at about 45,000 psi), it is evident that this material will perform well for all potential thrust forces exerted upon it by KST X15-755X. Aluminum survives with a large safety margin. PLA also performs well and survives with tensile values noted between 4,000-7,000 psi. Even at lower bounds, the pushrod remains structurally sound under direct tension.

However, compressive forces indicate a more critical limit - because with a slender rod, especially one unsupported for the approximate length of 10.16 in, Euler buckling will dictate compressive failure before yield. Thus, use of a pinned-pinned column buckling assessment states that an aluminum rod has a critical buckling load between 35 and 40 lbf dependent on exact length used (which is higher than any meaningful thrust force). Thus, within an operational flight scenario, the aluminum rod will not buckle under load. For a PLA rod, however, it has a far lower modulus of elasticity with a critical buckling threshold between 6 and 9 lbf - which is below any maximum compressive force exerted by the KST X15-755X. This signifies that a PLA pushrod will buckle before exceeding thrust torque conditions and thus, failure will occur through buckling - and not axial stress - which is why PLA should not be used for pushrod material on a flight critical system.

Finally, shear stress was examined in the clevis pins with a double-shear assumption per connection. Yet, even at maximum servo loading, predicted clevis pin shear stresses are well below industrial hardware tolerance capabilities - often exceeding 30,000 psi in steel - confirming that we need not worry about pin or bearing failures at these joints but instead focus on pushrod stability especially under compression.

Overall, internal results show that the aerodynamic forces imparted on the fins are well within the capabilities of actuation of KST X15-755X and additional internal loading from within the servo will define maximum loading within such a linkage. In terms of material selection, aluminum 6061-T6 offers excellent compressive and buckling resistance whereas PLA performs acceptable in tension but not in buckling. Therefore, aluminum is selected as the proper material for a final implementation of this active control mechanism's pushrod assembly component.

8.0 References:

[1] J. D. Anderson, Fundamentals of Aerodynamics, 6th ed. New York, NY, USA: McGraw-Hill, 2017.

[2] NASA Glenn Research Center, “Airfoil Lift and Drag Fundamentals,” NASA, 2020.

[3] NASA, “Standard Atmosphere Properties,” NASA, 2021.

[4] S. F. Hoerner, Fluid-Dynamic Lift. Brick Town, NJ, USA: Hoerner Fluid Dynamics, 1965.

[5] J. Barrowman, “The Barrowman Equations,” presented at NARAM-8, 1967.

[6] R. C. Hibbeler, Mechanics of Materials, 10th ed. Upper Saddle River, NJ, USA: Pearson, 2020.

[7] KST Servos, “X15-755X Datasheet,” 2024.

[8] Hitec RCD, “Servo Basics White Paper,” 2019.

[9] T. Torrado, M. Shemelya, E. D. Eckert, D. A. Artieri, and E. Greenway, “Mechanical properties of 3D-printed PLA,” J. Manuf. Process., vol. 20, pp. 1–5, 2015.

[10] R. G. Budynas and J. K. Nisbett, Shigley’s Mechanical Engineering Design, 11th ed. New York, NY, USA: McGraw-Hill, 2020.